MANCHESTER 1824
The University of Manchester

The University of Manchester Research

Silver assisted crack healing in SiC

DOI:
10.1016/j.actamat.2015.11.052

Document Version
Final published version

Link to publication record in Manchester Research Explorer

Citation for published version (APA):
Geng, X., Yang, F., Chen, Y., Lu, X., Zhong, X., & Xiao, P. (2016). Silver assisted crack healing in SiC. *Acta Materialia*, *105*(2), 121-129. https://doi.org/10.1016/j.actamat.2015.11.052

Published in:
Acta Materialia

Citing this paper
Please note that where the full-text provided on Manchester Research Explorer is the Author Accepted Manuscript or Proof version this may differ from the final Published version. If citing, it is advised that you check and use the publisher's definitive version.

General rights
Copyright and moral rights for the publications made accessible in the Research Explorer are retained by the authors and/or other copyright owners and it is a condition of accessing publications that users recognise and abide by the legal requirements associated with these rights.

Takedown policy
If you believe that this document breaches copyright please refer to the University of Manchester's Takedown Procedures [http://man.ac.uk/04Y6Bo] or contact uml.scholarlycommunications@manchester.ac.uk providing relevant details, so we can investigate your claim.

OPEN ACCESS

Download date:09. Jun. 2022

Acta Materialia 105 (2016) 121–129

Contents lists available at ScienceDirect

Acta Materialia

journal homepage: www.elsevier.com/locate/actamat

Full length article

Silver assisted crack healing in SiC

Xin Geng [a, b, *], Fan Yang [a], Yiqiang Chen [a, c], Xiaoxiao Lu [a], Xiangli Zhong [a], Ping Xiao [a, **]

[a] Materials Science Centre, School of Materials, The University of Manchester, Manchester M13 9PL, UK
[b] School of Materials Science and Engineering, Harbin Institute of Technology, Harbin 150001, People's Republic of China
[c] The Department of Materials Science and Engineering, Monash University, Clayton, VIC 3800, Australia

ARTICLE INFO

Article history:
Received 14 October 2015
Received in revised form
20 November 2015
Accepted 27 November 2015
Available online 24 December 2015

Keywords:
Silicon carbide
Silver
Reprecipitation
Crack healing

ABSTRACT

This paper provides a potential method through a dissolution-precipitation mechanism to achieve crack healing in SiC by a vacuum heat treatment with Ag at 1450 °C. The thermodynamic calculations and experimental results confirm that the Ag reacts with SiC to form a molten Ag–Si alloy and carbon, which accelerates material transport in SiC, and then by reaction between the Ag–Si and carbon, a new SiC is formed and fills inside the cracks and Vickers indentation impressions to achieve crack healing in SiC. The depth recovery ratio of the indentation is ~60%. The cracks underneath the indentation break into a row of isolated nodules, which is driven by reducing the interfacial energy between SiC and the Ag–Si alloy.

© 2015 Acta Materialia Inc. Published by Elsevier Ltd. All rights reserved.

1. Introduction

Silicon carbide (SiC) and its composites are important high temperature structural materials for gas turbines, and as nuclear fuel cladding materials, due to their superior mechanical properties (strength, hardness, and Young's modulus), low creep resistance at high temperature, low thermal expansion, good thermo-chemical stability and excellent irradiation tolerance property (low volumetric swelling of 0.7% after neutron irradiation at 1200 °C) [1–3]. However, it is susceptible to cracks caused by machining, friction, overloading, fatigue, *etc.*. Therefore, for its application at high temperature, SiC is required to maintain its structural integrity to improve the reliability, which raises an interest in the self-healing of the cracks.

Healing of cracks in SiC could be achieved by oxidation. Lange first reported an oxidation-induced crack healing in SiC at 1400 °C [4]. Under a dry air atmosphere, SiC reacts with oxygen (O_2) to form amorphous silica (SiO_2) and carbon monoxide (CO):

$$SiC(s) + \frac{3}{2}O_2(s) = SiO_2(l) + CO(g) \quad (1)$$

Healing of cracks is achieved due to not only the redistribution by the viscous flow of the glass phase, but also the volume expansion from SiC to SiO_2. The strength of SiC was reported to be fully recovered at room temperature [5–7]. However, it dropped dramatically to only half of its room temperature value at 600 °C [6] due to the softening of the glass phase SiO_2 at high temperatures [8]. Moreover, it should be pointed out that the oxidation method for crack healing in SiC is not applicable in the presence of water vapor, i.e., under the complex combustion environment for high-temperature turbine engines, as the water vapor causes volatility of SiO_2 by forming various gaseous species, e.g., $Si(OH)_4$, $SiO(OH)_2$, SiO(OH), *etc.* [9].

Re-sintering is another major crack healing mechanism for ceramics, in particular, oxide ceramics, in which cracks are healed through solid diffusion [10–13]. The required temperature to heal the cracks needs to exceed 0.7–0.9 of the melting point of single crystals or the sintering temperature of polycrystalline ceramics to induce grain growth (sapphire (single crystal Al_2O_3) ≥1800 °C, polycrystalline Al_2O_3 > 1400 °C and MgO>1600 °C) [14–17]. However, this mechanism is hardly applied to SiC due to the low diffusion coefficients and high activation energies of both Si and C even at high temperatures (1800–2350 °C) hindering the required long range Si and C atoms transport to heal cracks [18–21].

In this paper, we report a novel method to achieve crack healing

* Corresponding author. School of Materials Science and Engineering, Harbin Institute of Technology, Harbin 150001, People's Republic of China.
** Corresponding author. Materials Science Centre, School of Materials, The University of Manchester, Manchester M13 9PL, UK.
E-mail addresses: gengxin333@gmail.com (X. Geng), p.xiao@manchester.ac.uk (P. Xiao).

http://dx.doi.org/10.1016/j.actamat.2015.11.052
1359-6454/© 2015 Acta Materialia Inc. Published by Elsevier Ltd. All rights reserved.

in SiC governed by a dissolution-reprecipitation mechanism at a relatively low temperature (1450 °C).

2. Experimental procedure

2.1. Sample preparation

The fully-dense β-SiC bulk sample used in this study was provided by the Dow chemical company. It was fabricated by chemical vapor deposition (CVD) with a high purity of >99.9995%. The sample was cut into specimens with dimensions of 5 mm × 4 mm × 1 mm. One surface of the specimen was polished by standard metallographic procedures to a final polish using 25 nm colloidal silica suspensions, and then cleaned ultrasonically in water and dried in air. Cracks were generated on the polished surface by a Vickers micro-indenter using a load of 9.8 N with a dwell time of 10 s (Duramin microhardness tester, Struers, UK).

Ag powder (Alfa Aesar, A Johnson Matthey Co., Lancashire, UK, 99.9%, 0.7–1.3 μm) was cold pressed into a pellet (10 mm in diameter, 3–5 mm in thickness) under a uniaxial pressure of 100 MPa. The Ag pellet was placed on the indented surface of the SiC specimen and then the Ag/SiC couple was subjected to a vacuum heat treatment at 1450 °C for 48 h in a tube vacuum furnace (Elite Thermal Systems Ltd, Leicestershire, UK) with a heating and cooling rate of 300 °C/h. The vacuum level was maintained at ~10^{-5} mbar to avoid oxidation of the specimen.

2.2. Sample characterization

The microstructures evolution of SiC were observed by a scanning electron microscope (SEM) (FEI Quanta 650, Eindhoven, 8 kV, the Netherlands) and a transmission electron microscope (TEM, Tecnai™ G2 F30 U-TWIN, 300 kV, USA) coupled with an energy-dispersive X-ray spectrometer (EDX). The chemical compositions of the newly formed β-SiC and the Ag–Si nodules were quantitatively analyzed using EDX. A TEM sample and the cross-section under the indentation of the SiC after annealing with Ag were prepared by a focused ion beam (FIB; FEI Nova 600 Dual Beam System, USA).

The phase compositions were identified by Raman spectroscopy (Renishaw 1000, Gloucestershire, UK; 632.8 nm line of He–Ne laser), and the spectra were obtained from 200 to 4000 cm^{-1} with a laser beam of about 2 μm in diameter.

The depth profiles of the indentation impression along its diagonal direction were measured by a three dimensional non-contact surface mapping profiler (MicroXAM surface mapping microscope, Phase Shift Technologies, USA).

3. Results

3.1. Indentation recovery

Fig. 1(a) shows that the SiC grains on the polished surface have a typical columnar structure varying from 50 to 150 μm in length highlighted by the red dashed lines. Before heat treatment, the indentation impression shows a clear and sharp edge with a length of ~28 μm along the diagonal direction (Fig. 1(b)), and radial cracks are generated on the surface with a width of ~200 nm (Fig. 1(c)).

After vacuum heat treatment with Ag, a significant change in the morphology of the indentation impression is observed in Fig. 1(d). The indentation impression and the cracks are filled with newly-formed grains with fine sizes of 0.8–2 μm as shown in Fig. 1(e) and (f). The size of the indent remains almost unchanged, whereas the indent edges become irregular comparing with the sharp and clear edges before heat treatment.

Raman spectra collected from the surface and the indentation impression before and after heat treatment are shown in Fig. 2. Before heat treatment, the Raman spectrum of the un-indented surface (Fig. 2(a), curve I) shows two strong characteristic peaks centered at 796 and 972 cm^{-1}, which are attributed to the first order of transverse optical (TO) and longitudinal optical (LO) phonons of β-SiC [22,23]. Two additional weak peaks centered at 1524 and 1713 cm^{-1} represent the second-order Raman scattering of β-SiC [24–26]. The Raman spectrum of the indented region (Fig. 2(a), curve II) shows broadened peaks centered at below 500, around 600 and within the region from 700 to 1000 cm^{-1}, which are related to the structural damage caused by plastic deformation. This is in agreement with Ref. [27].

After a vacuum heat treatment with Ag, the Raman spectrum collected from the un-indented surface (Fig. 2(b), curve III) shows sharp peaks centered at 1330, 1584, 1618, 2472, 2662 and 3242 cm^{-1}, which are characteristic peaks of graphite [28]. No peaks corresponding to β-SiC are detected due to a strong signal of carbon in the Raman spectrum. On the contrary, the Raman spectrum of the indentation impression (Fig. 2(b), curve IV) shows not only the characteristic peaks from carbon, but also the two characteristic peaks from β-SiC.

The indentation impression after heat treatment with Ag was cross-sectioned along its diagonal by focused ion beam (FIB) milling as shown in Fig. 3(a). The indentation has been recovered by the newly-formed SiC grains. Fig. 3 (b) shows a color contrast of the SiC grains, due to the distribution of Ag impurity formed inside the newly-formed SiC, which is confirmed by the TEM analysis and will be discussed in detail in Section 3.2.

The effectiveness of healing was estimated by a recovery ratio, δ, defined as [29,30]:

$$\delta = \frac{(h_0 - h_a)}{h_0} \times 100\% \quad (2)$$

where h_0 and h_a are the maximum residual depths of the indentation impression before and after heat treatment with Ag, respectively.

The depth profiles of the Vickers indentations taken along the diagonal direction before and after heat treatment at 1450 °C are shown in Fig. 4. As shown in Fig. 4(a), after heat treatment with Ag, a significant change in the profilometric profile of the indentation impression could be observed. The maximum residual depth decreases from 2.74 μm before heat treatment to 1.07 μm after heat treatment. The recovery ratio calculated from Eq. (2) is 61%. For a comparison, one indented SiC sample was vacuum annealed without Ag at 1450 °C for 48 h (the morphologies of the indentation impressions before and after heat treatment are shown in Fig. S1 in the supplemental materials). The profilometric profiles of the indentation impression before and after heat treatment are almost identical as shown in Fig. 4(b). Therefore the comparison between Fig. 4(a) and (b) confirms the critical role of Ag in the indentation recovery of SiC.

In conclusion, the above observations indicate that after the vacuum heat treatment of SiC with Ag, carbon is formed on the surface and inside the indented impression. Moreover, new grains of β-SiC are formed to fill in the indentation impression and the radial cracks. The recovery ratio is 61.1%.

3.2. Crack healing

To reveal the cracks underneath the indentation impression before heat treatment, the fracture surface along the diagonal direction was prepared by a three-point bending test. Fig. 5(a) and (b) show that the length of a median crack in the fracture surface is

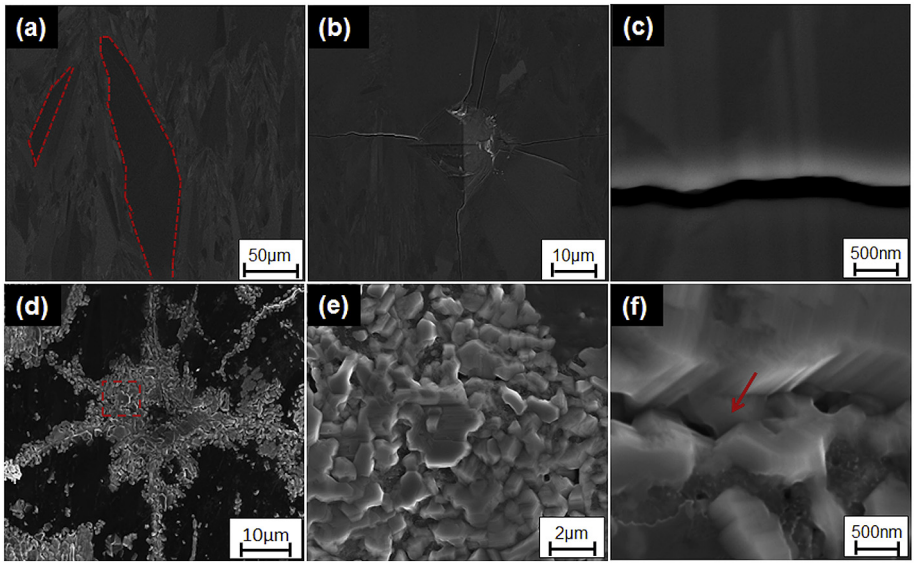

Fig. 1. SEM images obtained from the SiC surface and indentation impression before and after vacuum heat treatment with Ag. Before heat treatment: (a) surface morphology, the grains are highlighted by red dashed lines; (b) a typical Vickers indentation impression; (c) a high magnification image of a radial crack of Fig. 1(b); After heat treatment: (d) a Vickers indentation impression; (e) a high magnification image for the newly formed grains filling inside the indentation impression of the red rectangular area in Fig. 1(d); (f) a high magnification image of a healed crack of Fig. 1(d). (For interpretation of the references to colour in this figure legend, the reader is referred to the web version of this article.).

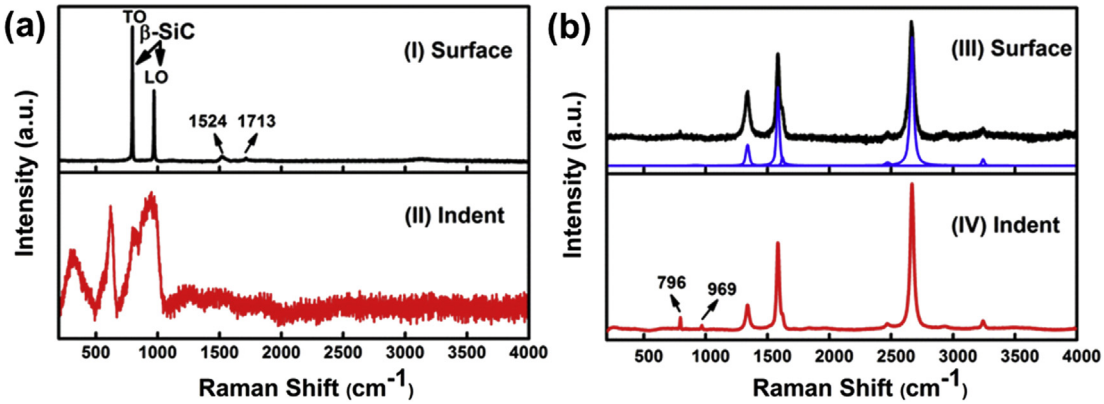

Fig. 2. Raman spectra taken from the SiC surface and indent impression before and after vacuum heat treatment with Ag. (a) Before heat treatment: spectrum (I) taken from the polished surface; spectrum (II) taken from the indentation impression; (b) After heat treatment: spectrum (III) taken from the surface; and spectrum (IV) are taken from the indentation impression.

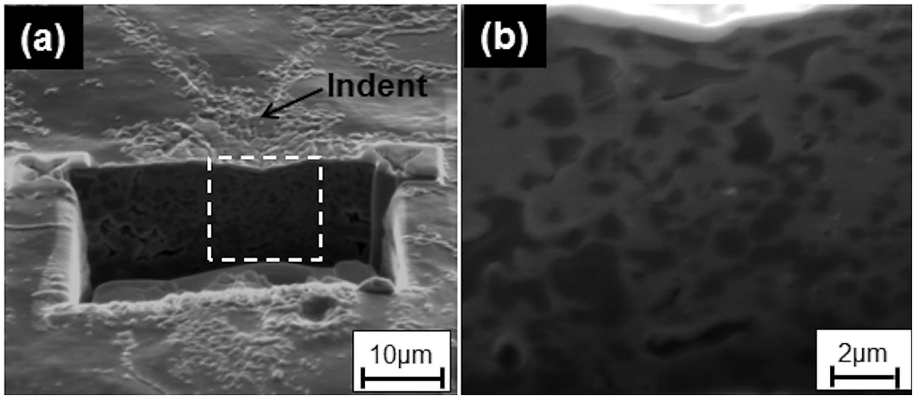

Fig. 3. Morphologies underneath the center of the indentation impression after heat treatment with Ag revealed by FIB milling: (a) a cross sectional SEM image; (b) a high magnification image of the white rectangular area in Fig. 3(a).

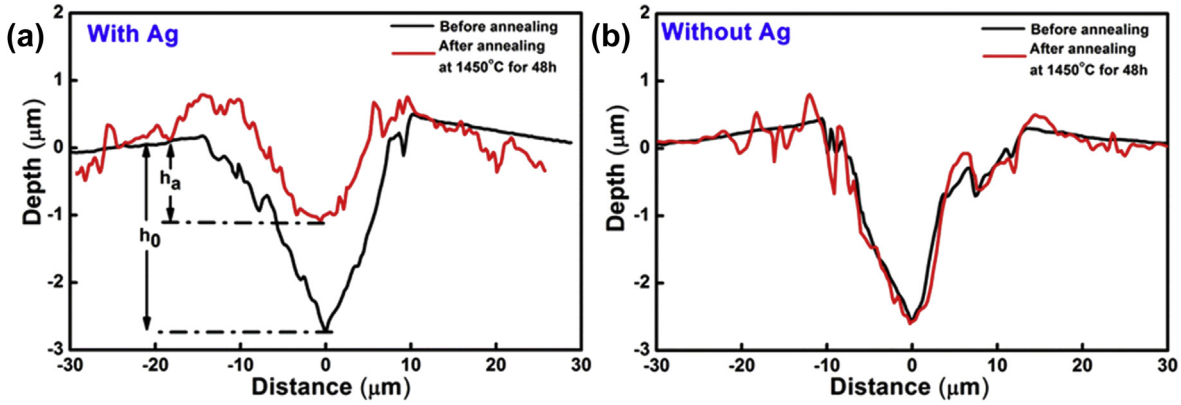

Fig. 4. Line scan profiles taken along the diagonal direction of indentation impressions: (a) before and after heat treatment with Ag; (b) before and after heat treatment without Ag.

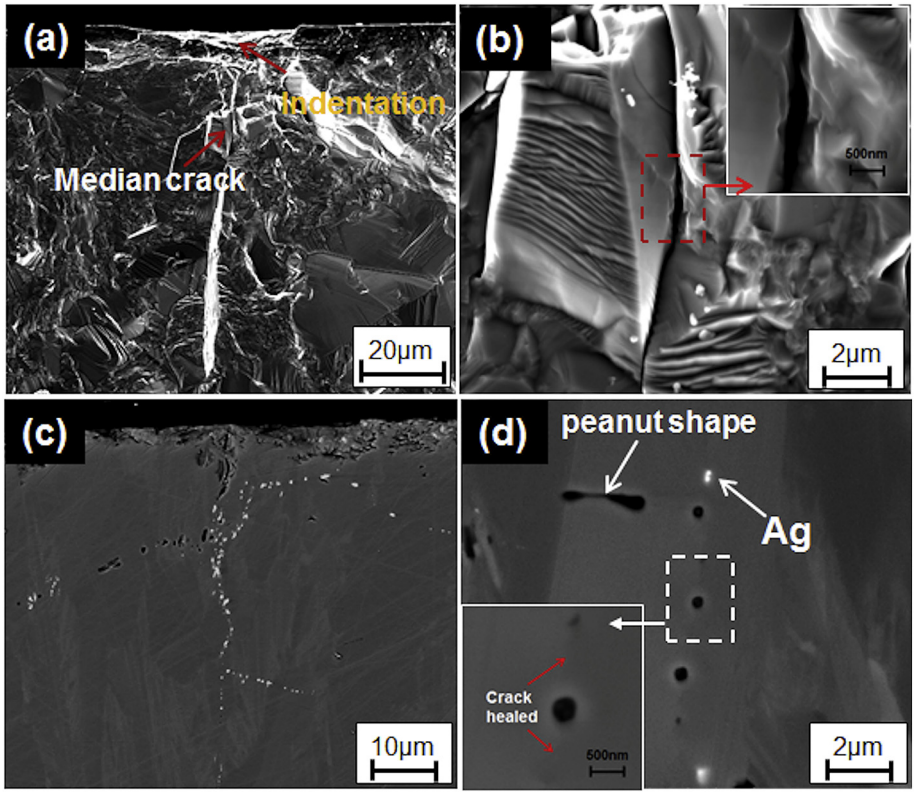

Fig. 5. SEM micrographs of cracks underneath the indentation impression before and after vacuum heat treatment with Ag. Before heat treatment: (a) a cross-sectional fracture surface image showing pristine median and lateral cracks; (b) a high magnification image of the median crack of Fig. 5(a), the inset image indicates the crack surface morphology of the red rectangular area in Fig. 5(b); After heat treatment: (c) a polished cross-sectional image showing the healed median and lateral cracks; (d) a high magnification image of the median crack of Fig. 5(c); the inset image indicates the voids morphology of the white rectangular area in Fig. 5(d). (For interpretation of the references to colour in this figure legend, the reader is referred to the web version of this article.).

approximately 80 μm and the width is about 500 nm. A high magnification image of the median crack shows that the crack surface is rough (Fig. 5(b)). For a comparison, the cross section of the SiC sample was carefully polished until the center of the indentation impression after heat treatment with Ag. As shown in Fig. 5(c), the original profiles of the median and the lateral cracks are sketched by discontinuous Ag nodules and voids (voids were formed during the polishing process due to the extrusion or dissolution of Ag by the silica suspension). Fig. 5(d) illustrates that Ag exists in the cracks of SiC with two morphologies: a 'peanut' shape and an isolated spherical shape. A high magnification image of the area near the Ag nodules (voids) shows that the crack has been fully healed (the inset image of Fig. 5(d)). It is worth noticing that the surface inside the voids is smooth compared with the tortuous surface inside the pristine median crack (Fig. 5(d)). At high temperature, the melted Ag penetrates through the crack and fills the crack gap. The Ag liquid breaks into a row of nodules due to a capillarity-induced shape change to reduce the interfacial energy [12]. In the meantime, the dissolution-reprecipitation process occurs. The gaps between two Ag nodules are filled by newly-formed SiC grains. This mechanism will be discussed in detail in Section 4.3.

FIB was used to prepare a TEM sample from the healed median crack region on the cross-sectional polished surface (Fig. 6(a)). The TEM sample contains two isolated spherical shape Ag–Si nodules.

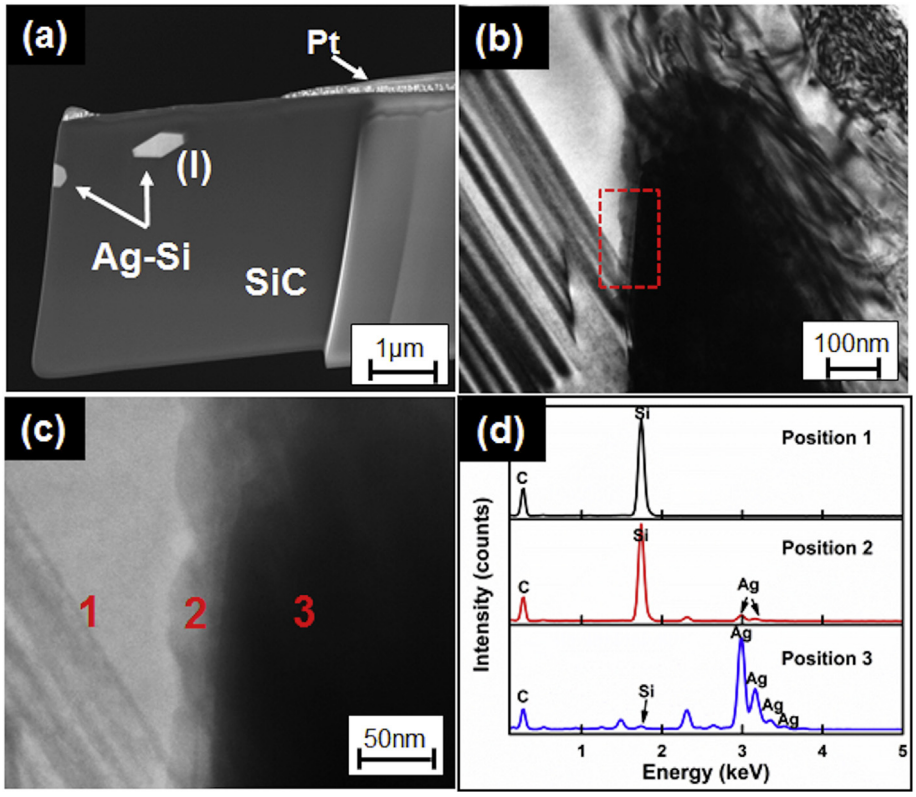

Fig. 6. TEM analysis of the morphology and composition of phases formed inside the median crack after vacuum annealing with Ag: (a) a SEM image for the TEM sample; (b) a bright field image for nodule (I) in Fig. 6(a); (c) a high magnification image of the red rectangular region in Fig. 6(b); (d) EDX analysis of regions 1, 2 and 3 of Fig. 6(c). (For interpretation of the references to colour in this figure legend, the reader is referred to the web version of this article.).

The bright field TEM image of the Ag–Si nodule (I) (Fig. 6(b)) shows that an additional layer is formed between the pristine SiC and the Ag–Si nodule, as illustrated by the color difference among the three regions. Moreover, the interface is smooth between the Ag–Si nodule and this newly formed additional layer (Fig. 6(c)), which the newly-formed phase smooths the tortuous pristine crack surface of the SiC. Point EDX analysis (Fig. 6(d)) reveals that the brighter area (position 1) contains only Si and C, corresponding to the original SiC. The interfacial layer (position 2) contains Si, C and Ag, corresponding to the newly-formed SiC. It is confirmed that the contrast difference comes from the Ag impurity dissolved in the newly-formed SiC grains, which is in agreement with the results reported by Sawyer and Page [31]. Moreover, an EDX spectrum of the nodule (position 3) indicates that Si dissolves in the Ag nodule. It should be noted that the electron beam size is sufficiently small (<1 nm) to guarantee that all the information is collected from the each region without influences from the others.

In summary, cracks underneath the indentation impression of SiC are healed by breaking up to rows of 'peanut' and isolated spherical shape Ag–Si nodules after the vacuum heat treatment with Ag at 1450 °C. New SiC is formed to fill the gaps between the nodules in the cracks, and smooth the tortuous crack surface of SiC.

4. Discussion

The above observations indicate that after the vacuum heat treatment of SiC with Ag: 1) the indentation impression and the cracks are healed by newly-formed β-SiC grains, and carbon is formed on the surface and on the indented impression; 2) both the 'peanut' and spherical shape of the Ag–Si nodules formed and stretched the cracks during the isothermal heat treatment. In the following, thermodynamic and kinetics aspects of cracks healing in SiC with the assistance by silver (Ag) will be discussed. Firstly, enhancement of material transport (Si) in SiC achieving crack healing of SiC at low temperature (1450 °C) will be discussed by the thermodynamic calculation of the reaction between Ag and SiC (present in Section 4.1). Secondly, the driving force for the indentation recovery by filling with the reprecipitation fine β-SiC grains is discussed in Section 4.2. Finally, the kinetics model for crack (the median and the lateral cracks) healing and Ag–Si alloys nodules evolution behaviors is presented in Section 4.3.

4.1. Enhancement of material transport in SiC by annealing with Ag

It is difficult to heal the cracks and recover micro-indentation impressions of SiC governed by the re-sintering mechanism annealed at low temperature (1450 °C), since the activation energies for Si or C self-diffusing through SiC are high: >695 kJ/mol for Si and >562 kJ/mol for C [18–21,32]. The slow solid state diffusion process cannot satisfy the long range material transport for healing the cracks. In the following, thermodynamic calculation is employed to discuss that the addition of Ag changes the Si transport way from solid diffusion to a liquid Ag–Si alloy flow, similar to how silica glass phase filled the cracks in SiC caused by the oxidation process. The liquid Ag–Si alloy flow accelerates crack healing process.

Firstly, the liquid of Si cannot be generated spontaneously by purely the decomposition of SiC as shown in Eq. (3):

$$SiC(s) \rightarrow Si(l) + C(s) \tag{3}$$

$$\Delta G_1 = \sum x_i \cdot \mu_i^0 = \mu_{Si}^0 + \mu_C^0 - \mu_{SiC}^0 \quad (4)$$

where ΔG_1 is the Gibbs energy of reaction (3); μ_{SiC}^0 (-1.6561 × 10^5 J/mol),μ_{Si}^0 (-7.1517 × 10^4 J/mol) and μ_C^0 (-3.520 × 10^4 J/mol) are the chemical potential of SiC, Si and C at 1450 °C. The values are determined by commercial software (Thermo-Calc 4.1, database: NUCL 10).

The positive value of $\Delta G_1 = 5.89 \times 10^4$ J confirms that reaction (3) cannot occur spontaneously at 1450 °C.

In contrast, SiC annealing with Ag at 1450 °C helps to form liquid Ag–Si alloys. Our previous study has found the following reversible chemical reaction between Ag and SiC at 1450 °C in vacuum [33]:

$$(1\text{-}x)\cdot Ag(l) + x\cdot SiC(s) \leftrightarrow Ag_{1-x}Si_x(l) + x\cdot C(s) \quad (5)$$

where x represents the mole fraction of silicon (Si) in liquid silver-silicon alloys.

According to the silver-silicon phase diagram [34], the experimental temperature (1450 °C) is higher than the melting points of all silver-silicon alloys, which is in the range from 835 to 1414 °C. Ag, in its liquid form, reacts with SiC at 1450 °C to form carbon and a Si–Ag alloy. Subsequently, reprecipitation of β-SiC occurs inside the Vickers micro-indentations and heals the cracks. Furthermore, the Ag–Si alloy evaporates at high temperature, leaving carbon and new SiC grains.

Gibbs free energy (ΔG_2) of reaction (5) in the right direction is calculated as shown in Eq. (6):

$$\Delta G_2 = \sum x_i \cdot \mu_i^0 = \mu^0_{Ag_{(1-x)}-Si_{(x)}} + x\cdot\mu_C^0 - (1-x)\cdot\mu_{Ag}^0 - x\cdot\mu_{SiC}^0 \quad (6)$$

The regular solution model is employed to derive the chemical potential of the molten Ag–Si alloys:

$$\mu^0_{Ag_{(1-x)}-Si_{(x)}} = (1-x)\cdot\mu_{Ag}^0 + x\cdot\mu_{Si}^0 + RT\cdot\left((1-x)\cdot\ln\alpha_{Ag} + x\cdot\ln\alpha_{Si}\right) \quad (7)$$

where α_{Ag} and α_{Si} are the activities of Si and Ag in a molten Ag–Si alloy at the given silicon composition (x). Substituting Eq. (7) in Eq. (6), the expression can hence be written as:

$$\Delta G_2 = x\cdot\left(\mu_{Si}^0 + \mu_C^0 - \mu_{SiC}^0\right) + RT\cdot\left((1-x)\cdot\ln\alpha_{Ag} + x\cdot\ln\alpha_{Si}\right) \quad (8)$$

The Gibbs energy of the reversible reaction (5) in the right direction can be divided into two terms:$A = x\cdot(\mu_{Si}^0 + \mu_C^0 - \mu_{SiC}^0)$ and $B = RT\cdot((1-x)\cdot\ln\alpha_{Ag} + x\cdot\ln\alpha_{Si})$;

It is clear that term A represent x multiplied by the Gibbs energy (ΔG_1) of reaction (3), of which the value is positive. The activities of silver (α_{Ag}) and silicon (α_{Si}) in molten Ag–Si alloys depending on the silicon mole fraction (x) at 1450 °C were determined by the Thermo-Calc software (version 4.1 and NUCL 10 database) and plotted in Fig. 7(a), of which the values are in agreement with the experimental values measured by Robinson [35]. It should be noted that the activities of Ag (α_{Ag}) and Si (α_{Si}) are lower than 1 at any composition, where $\ln\alpha_{Ag}<0$ and $\ln\alpha_{Si}<0$, therefore, the value of term B is negative and helps to reduce the value of ΔG_2. The relationship between ΔG_2 and the silicon mole fraction (x) is shown in Fig. 7(b). The definition of the threshold silicon fraction (m_t) is the silicon mole fraction corresponding to $\Delta G_2 = 0$ (m_t = 1.203 at% for Fig. 7(b)). It confirms that annealing with Ag causes SiC decomposition to liquid Ag–Si alloys and carbon for a Si mole fraction lower than 1.203 at%, and therefore, the molten Ag–Si alloys accelerate material transport in SiC compared with solid diffusion.

In the meantime, silver in the Ag–Si alloy evaporates during the isothermal heat-treatment process at 1450 °C, which increases the silicon mole fraction in the Ag–Si alloys. When the silicon mole fraction exceeds the threshold silicon fraction value (m_t = 1.203 at %), the reaction (5) occurs spontaneously in the reverse direction, new β-SiC grains are reprecipitated and fill the Vickers micro-indentations and the cracks by the reaction of Ag–Si alloys and carbon.

In conclusion, the dissolution-reprecipitation mechanism governs indentation recovery and cracks healing in SiC by the assistance with Ag annealed at 1450 °C, due to formation of the molten Ag–Si alloys. Moreover, following the direction of thermodynamic calculation of reaction (5), the prerequisites for choosing other metals, which could assist cracks healing in SiC, are summarized below:

(1) The melting points of both metal and metal-Si alloys are low (<1450 °C).
(2) The liquid metals can dissolve an amount of silicon, but do not form an intermetallic compound.
(3) The activities of silicon and metals in the liquid metal-Si alloys are lower than 1.

In the following section, the driving force for the reprecipitation fine β-SiC grains filling the Vickers micro-indentation will be discussed.

4.2. SiC reprecipitation for indentation recovery

The local interface curvature affected the Gibbs energy of SiC, as expressed below [36]:

$$\mu_{SiC} = \mu_{SiC}^0 \pm \gamma\cdot\Omega\cdot\kappa \quad (9)$$

where μ_{SiC} is the Gibbs potential of SiC (J/mol); μ_{SiC}^0 is the chemical potential of SiC (J/mol); γ is the surface tension of SiC (J/m^2); The surface tension of SiC is $\gamma = 3.0-0.546 \times 10^{-3}$ T (J/m^2, T is absolute temperature (K)) [37]; Ω is the SiC atomic volume (1.25 × 10^{-2} m^3/mol); κ is the local curvature of the SiC surface, '+' for the convex surface and '–' for the concave surface.

There are two principle curvatures at each point of the indentation impression: κ_1 corresponding to along the x-y axis and κ_2 is normal to the x-y axis. The mean curvature $\kappa = \kappa_1 + \kappa_2$. It can be considered that a Vickers indentation impression is constituted of a series of thin slice as shown in Fig. 8(a) (slice (I), (II), (III) *etc.*), where each slice is highlighted by one color. Since the thickness of each slice is thin and can be consider as flat, the curvature κ_2 is 0. Therefore, the mean curvature (κ) corresponding to the surface of each slice equals the curvature (κ_1) of the depth profile. The depth profile of the Vickers indentation impression along its diagonal direction has been used as an example to calculate the curvatures (the black line shown in Fig. 8(b)). A ninth-order polynomial function, $f(x) = \sum_{i=0}^{9} p_i \cdot x^i$, is used to fit this depth profile as shown in the red curve in Fig. 8(b) and the parameters (p_i) of this function are determined by commercial software (Matlab R2009a). The curvatures of the fitted depth profile (the red curve in Fig. 8(b)), κ, along the distance can be calculated using the following equation.

$$\kappa = \frac{|f''(x)|}{\left(1 + f\prime(x)^2\right)^{3/2}} \quad (10)$$

The relationship between the curvatures of the depth profile of Fig. 8(b) and distance is plotted in Fig. 8(c). The curvature values

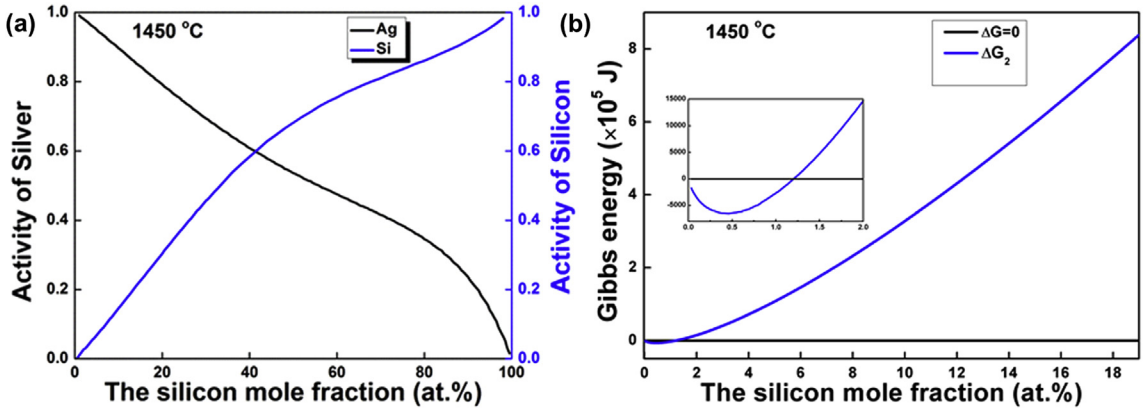

Fig. 7. Thermodynamic calculation of the reaction between Ag and SiC at 1450 °C: (a) the relationship between activities of both Ag and Si in molten Ag–Si alloys and the silicon mole fraction; and (b) the relationship between Gibbs energy of the reaction and the silicon mole fraction (x), the inset image indicates an enlarged view for x from 0 to 2.

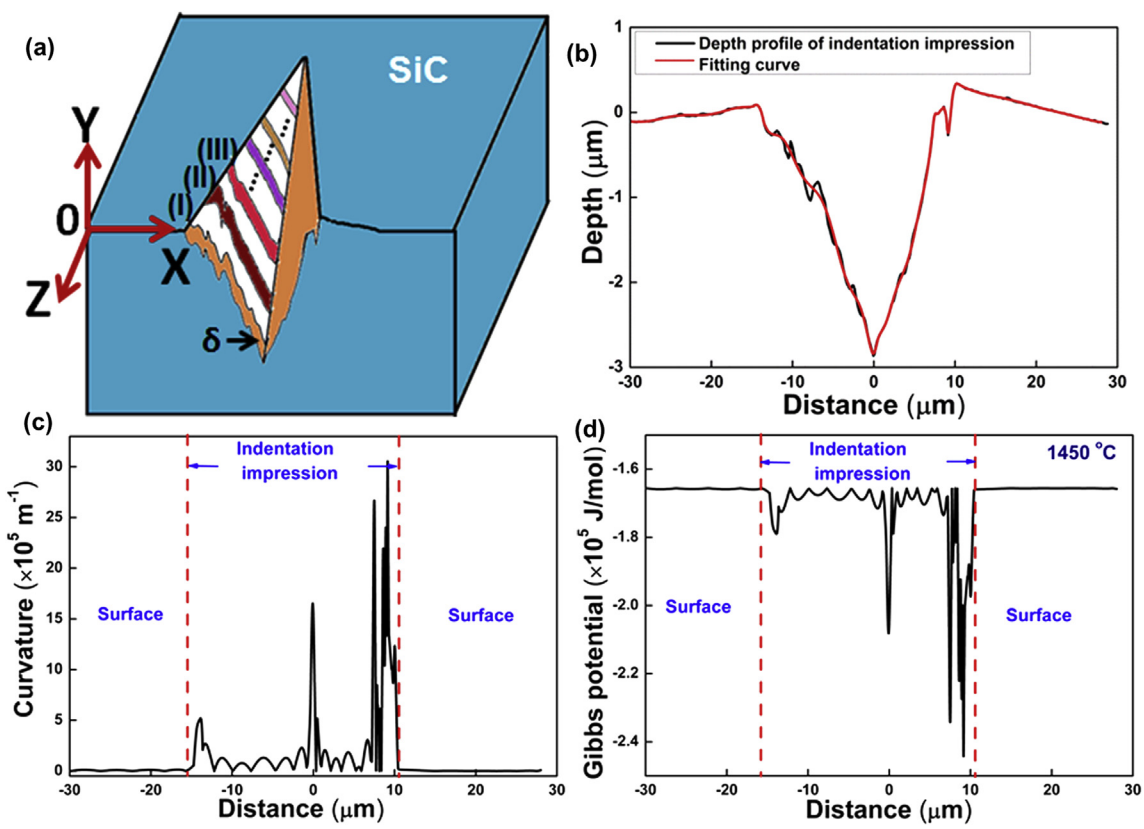

Fig. 8. (a) Schematic illusion of the SiC Vickers indentation geometry constituted by serial slices; (b) line scan profiles taken along the diagonal direction of an indentation impression and its ninth-order polynomial functional fitting curve; (c) a plot of the curvature of the line scan profile of Fig. 8(b) as a function of distance; and (d) a plot of Gibbs potential of SiC versus distance.

inside the indentation impression range from 585 to 3×10^6 m^{-1} and its values are much larger than them on the surface, especially at the indentation edge and center area. Therefore, the SiC Gibbs potential corresponding to the depth profile of Fig. 8(b) at 1450 °C calculated by Eq. (9) versus the distance is plotted in Fig. 8(d). This suggests that the Gibbs potential of SiC inside the indentation impression (concave surface) is less than that on the flat surface.

The Gibbs free energy (ΔG_3) of reaction (5) occurring inside the indentation is shown below:

$$\Delta G_3 = x\cdot\left(\mu^0_{Si} + \mu^0_C - \mu^0_{SiC} + \gamma\cdot\Omega\cdot\kappa\right) + RT\cdot\left((1-x)\cdot\ln\alpha_{Ag} + x\cdot\ln\alpha_{Si}\right) \quad (11)$$

Fig. 9(a) shows a surface plot of ΔG_3 versus silicon mole fraction (x) and distance (flat surface to the indentation impression to flat surface, corresponding to Fig. 8). It suggests that both the silicon mole fraction (x) and curvature affect significantly on the values of ΔG_3. The 2-D plot of the threshold silicon fraction (m_t) versus distance is shown in Fig. 9(b), where $\Delta G_3 = 0$.

Due to the high curvature values of the indentation impression,

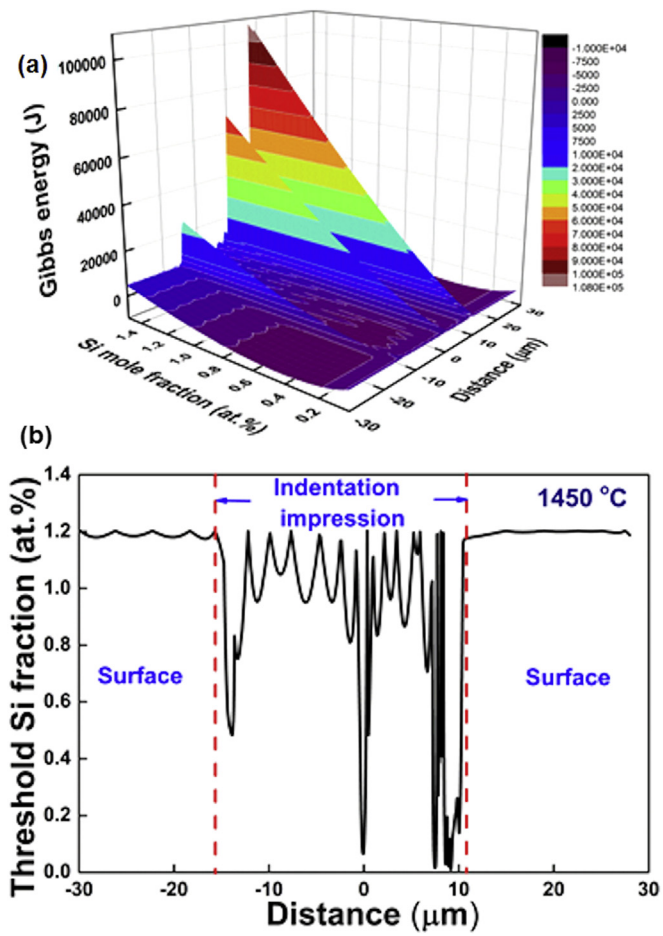

Fig. 9. Thermodynamic calculation of the reaction between Ag and SiC Vickers indentation impression at 1450 °C: (a) plots of Gibbs energy change versus silicon mole fraction (x) and distance; (b) the relationship between the threshold silicon fraction and distance.

the gradient of the threshold silicon fraction values (m_t) causes the fine β-SiC grains to be preferentially reprecipitated inside the indentation impression especially at the edges and center of the indentation. With silver in Ag–Si alloys evaporation during the isothermal process, it is easier to reach the threshold silicon fraction values (m_t) inside the indentation compared with the flat surface, and then the reversible reaction (5) occurs spontaneously in the reverse direction. This is in agreement with the depth profile result that the height of the indentation impression edge is higher than the height of the flat surface after the vacuum heat-treatment with Ag (shown in the red curve in Fig. 4(a)).

In summary, the existence of a gradient in the Gibbs potential of SiC ($\gamma\cdot\Omega\cdot\kappa$ (J/mol), where the Gibbs potential at the flat surface is higher than the value at the concave surface (the Vickers indentation), drives the SiC transport in the direction from the flat surface region to the indentation impression region by reducing the system Gibbs energy of SiC. Therefore, the driving potential is $\gamma\cdot\Omega\cdot\kappa$ (J/mol), in a direction from the flat surface to the Vickers indentation impression of SiC.

4.3. Interfacial tension induced Ag–Si nodules inside cracks of SiC

After the heat-treatment with Ag at 1450 °C, SEM and TEM micrographs illustrated that the cracks underneath the SiC surface were sketched by both 'peanut' shape and isolated Ag–Si nodules. The newly-formed β-SiC not only fully healed the gaps between two Ag–Si nodules, but also created an additional layer between an Ag–Si alloy nodule and pristine SiC crack surface. Similar phenomena that cracks break up into rows of isolated spherical voids are found in Al_2O_3, MgO and related ceramics by annealing at elevated temperatures [16,17,38,39].

The Plateau-Rayleigh instability theory [40] is employed to explain the mechanism for the evolution of the isolated Ag–Si nodules inside the cracks of SiC, and a model is proposed as shown in Fig. 10. Initially, capillarity and gravity forces drive the molten Ag filling in the cracks of SiC (Fig. 10(a)). The 'perturbations' as shown in areas (I) and (II) of Fig. 10(a) are a schematic illustration of a pristine rough median crack surface in SiC as depicted in Fig. 5(a) and (b). In the 'perturbations' areas, the interfacial tension between molten Ag and SiC, $\mathbf{F} = \gamma_{SL}$, breaks into two vectors: $\boldsymbol{F_a}$ along the crack direction and $\boldsymbol{F_v}$ normal to that and points to the molten Ag. Therefore, the normal vector $\boldsymbol{F_v}$ "drags" the unstable continuous molten silver inside the crack to form the 'peanut' shape Ag–Si alloys nodules as shown in Fig. 10(b). In the meantime, the reaction between molten silver and SiC occurs and a flux of SiC is transported from the trough to the crest inducing by a gradient of the SiC Gibbs potential, due to the curvature difference as investigated in Section 4.2. Therefore, the isolated Ag–Si nodules are formed and the cracks between those nodules are fully healed as shown in Fig. 10(c).

In summary, Cracks underneath the SiC surface tends to break up rows of the isolated spherical Ag–Si nodules governed by minimizing interfacial surface. The projected force of interfacial tension between molten Ag or Ag–Si alloys and SiC ($\boldsymbol{F_v}$) is the driving force for healing the cracks in SiC. Moreover, this driving force tends to smooth the interface between the SiC crack surface and the Ag–Si alloy nodules.

5. Conclusions

In summary, Vickers indentation impression and cracks in SiC could be healed by a vacuum heat treatment with Ag through a dissolution-reprecipitation mechanism. At high temperature, liquid Ag reacts with SiC to form carbon and an Ag–Si alloy, followed by a reprecipitation process of SiC. The newly-formed SiC grains healed the cracks and recovered the indentation impression. The recovery

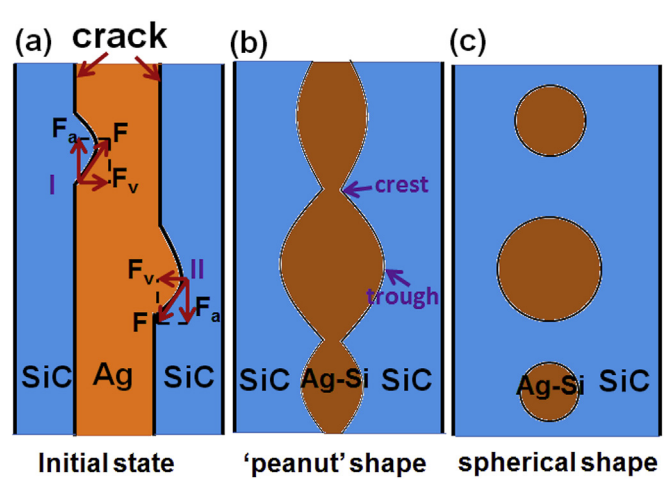

Fig. 10. Schematic illustration of the morphological evolution of the Ag–Si alloy nodules with Rayleigh instabilities: (a) Initial state, 'perturbation'; (b) 'peanut' shape nodules of Ag–Si alloys formed driven by the interfacial tension between Ag–Si alloys and SiC; and (c) final break up into rows of spherical Ag–Si alloys nodules by minimizing the interface.

ratio of the indentation impression is ~60%. A thermodynamic calculation confirms that the formation of Ag–Si alloys accelerates materials transport in SiC in order to heal the damage areas at 1450 °C. Moreover, a gradient in the SiC Gibbs potential between the flat surface and the concave surface (indentation impression) drives the newly-formed SiC grains to precipit inside the indentation impression by reducing the Gibbs energy of the SiC sample. A model based on the Plateau-Rayleigh instability theory is proposed to explain the morphological evolution of isolated Ag–Si nodules by minimizing the interfacial energy between SiC and Ag–Si alloys.

Acknowledgment

The authors would like to thank Professor B. Ralph for proofreading the manuscript. X. Geng wants to thank China Scholarship Council (CSC) for providing the funding.

Appendix A. Supplementary data

Supplementary data related to this article can be found at http://dx.doi.org/10.1016/j.actamat.2015.11.052.

References

[1] L.L. Snead, T. Nozawa, Y. Katoh, T.S. Byun, S. Kondo, D.A. Petti, Handbook of SiC properties for fuel performance modeling, J. Nucl. Mater 371 (2007) 329–377.
[2] G. Liu, J. Li, Y. Shan, J. Xu, Highly dense β-SiC ceramics with submicron grains prepared by sintering of nanocrystalline powders, Scr. Mater 67 (2012) 416–419.
[3] R. Naslain, Design, preparation and properties of non-oxide CMCs for application in engines and nuclear reactors: an overview, Compos. Sci. Technol. 64 (2004) 155–170.
[4] F. Lange, Healing of surface cracks in SiC by oxidation, J. Am. Ceram. Soc. 53 (1970) 290, 290.
[5] J. Korouš, M.C. Chu, M. Nakatani, K. Ando, Crack healing behavior of silicon carbide ceramics, J. Am. Ceram. Soc. 83 (2000) 2788–2792.
[6] S.K. Lee, W. Ishida, S.Y. Lee, K.W. Nam, K. Ando, Crack-healing behavior and resultant strength properties of silicon carbide ceramic, J. Eur. Ceram. Soc. 25 (2005) 569–576.
[7] Y.W. Kim, K. Ando, M.C. Chu, Crack-healing behavior of liquid-phase-sintered silicon carbide ceramics, J. Am. Ceram. Soc. 86 (2003) 465–470.
[8] K.W. Nam, J.S. Kim, S.W. Park, The high temperature strength of SiC ceramics based on SiO_2 nano-colloidal employed, Mat. Sci. Eng. A 527 (2010) 5400–5404.
[9] E.J. Opila, J.L. Smialek, R.C. Robinson, D.S. Fox, N.S. Jacobson, SiC recession caused by SiO_2 scale volatility under combustion conditions: II, thermodynamics and gaseous-diffusion model, J. Am. Ceram. Soc. 82 (1999) 1826–1834.
[10] M. Mitomo, T. Nishimura, M. Tsutsumi, Crack healing in silicon nitride and alumina ceramics, J. Mat. Sci. Lett. 15 (1996) 1976–1978.
[11] A. Evans, E. Charles, Strength recovery by diffusive crack healing, Acta Metall. Mater. 25 (1977) 919–927.
[12] T.K. Gupta, Instability of cylindrical voids in alumina, J. Am. Ceram. Soc. 61 (1978) 191–195.
[13] D.L. Smith, B. Evans, Diffusional crack healing in quartz, J. Geophys. Res Sol. Ea. (1978–2012) 89 (1984) 4125–4135.
[14] W. Nakao, K. Takahashi, K. Ando, Self-healing of surface cracks in structural ceramics, Adv. Nanomater. (2010) 555–593.
[15] P. Greil, Generic principles of crack-healing ceramics, J. Adv. Ceram. 1 (2012) 249–267.
[16] J. Rödel, A.M. Glaeser, High-temperature healing of lithographically introduced cracks in sapphire, J. Am. Ceram. Soc. 73 (1990) 592–5601.
[17] T. Gupta, Kinetics of strengthening of thermally shocked MgO and $A1_2O_3$, J. Am. Ceram. Soc. 59 (1976) 448–449.
[18] M. Hon, R. Davis, Self-diffusion of ^{14}C in polycrystalline β-SiC, J. Mat. Sci. 14 (1979) 2411–2421.
[19] M. Hon, R. Davis, D. Newbury, Self-diffusion of ^{30}Si in polycrystalline β-SiC, J. Mat. Sci. 15 (1980) 2073–2080.
[20] J. Hong, R.F. Davis, Self-diffusion of carbon 14 in high-purity and N-doped α-SiC single crystals, J. Am. Ceram. Soc. 63 (1980) 546–552.
[21] J. Hong, R.F. Davis, D. Newbury, Self-diffusion of silicon-30 in α-SiC single crystals, J. Mat. Sci. 16 (1981) 2485–2494.
[22] S.I. Nakashima, H. Harima, Raman investigation of SiC polytypes, Phys. Status Solidi A 162 (1997) 39–64.
[23] Z. Feng, A. Mascarenhas, W. Choyke, J. Powell, Raman scattering studies of chemical-vapor-deposited cubic SiC films of (100) Si, J. Appl. Phys. 64 (1988) 3176–3186.
[24] D. Olego, M. Cardona, Pressure dependence of Raman phonons of Ge and 3C-SiC, Phys. Rev. B 25 (1982) 1151.
[25] Z. Feng, Second order Raman scattering of cubic silicon carbide, Sci. Access 2 (2004) 242–243.
[26] J. Burton, L. Sun, F. Long, Z. Feng, I. Ferguson, First-and second-order Raman scattering from semi-insulating 4H-SiC, Phys. Rev. B 59 (1999) 7282.
[27] G. Chollon, J. Vallerot, D. Helary, S. Jouannigot, Structural and textural changes of CVD-SiC to indentation, high temperature creep and irradiation, J. Eur. Ceram. Soc. 27 (2007) 1503–1511.
[28] A.C. Ferrari, J. Robertson, Raman Spectroscopy in Carbons: From Nanotubes to Diamond, Royal Soc., 2004.
[29] W. Ni, Y.T. Cheng, D.S. Grummon, Recovery of microindents in a nickel-titanium shape-memory alloy: a "self-healing" effect, Appl. Phys. Lett. 80 (2002) 3310–3312.
[30] W. Huang, J. Su, M. Hong, B. Yang, Pile-up and sink-in in micro-indentation of a NiTi shape-memory alloy, Scr. Mater 53 (2005) 1055–1057.
[31] G. Sawyer, T. Page, Microstructural characterization of "REFEL" (reaction-bonded) silicon carbides, J. Mat. Sci. 13 (1978) 885–904.
[32] R.N. Ghoshtagore, R. Coble, Self-diffusion in silicon carbide, Phys. Rev. B 143 (1966) 623.
[33] X. Geng, F. Yang, N. Rohbeck, P. Xiao, An original way to investigate silver migration through silicon carbide coating in TRISO particles, J. Am. Ceram. Soc. 97 (2014) 1979–1986.
[34] R. Olesinski, A. Gokhale, G. Abbaschian, The Ag–Si (silver-silicon) system, J. Phase Equilib. 10 (1989) 635–640.
[35] V.S. Robinson, S.K. Tarby, Thermodynamic properties of liquid Ag–Si alloys, Metall. Trans. 2 (1971) 1347–1350.
[36] R.W. Balluffi, S. Allen, W.C. Carter, Kinetics of Materials, John Wiley & Sons, 2005.
[37] R.H. Bruce, Science of Ceramics, in: G.H. Stewart (Ed.), British Ceramic Society Conference, London, 2, 1965, p. 359.
[38] T. Gupta, Crack healing in Al_2O_3, MgO, and related materials, Adv. Ceram. 10 (1984) 750.
[39] C. Yen, R. Coble, Spheroidization of tubular voids in Al_2O_3 crystals at high temperatures, J. Am. Ceram. Soc. 55 (1972) 507–509.
[40] J.W. Strutt, L. Rayleigh, On the instability of jets, Proc. Lond. Math. Soc. 10 (1878) 4–13.